MSc Thesis

3D Lattice Analysis of Cement Paste

Zhiwei Qian

Delft University of Technology

April 2008

The purpose of computing is insight, not numbers.
– R. W. Hamming

... but for the student,
numbers are often the best road to insight.
– A. Ralston

Acknowledgements

First of all, I would like to express my gratitude to Prof. dr. ir. Klaas van Breugel who gave me the admission to study here at TU Delft in 2005.

I appreciate my daily supervisors Dr. Guang Ye and Dr. ir. Erik Schlangen for their kind supervisions and discussions throughout the research.

Dr. ir. Pierre Hoogenboom from structural mechanics group is also appreciated for his valuable comments on the project.

The coordinator for Structural Engineering track Ir. Lambert Houben managed the issues concerning graduation.

During the study, Ir. Jian Zhou provided some interesting ideas and helped me to complete my thesis.

I would like to thank my colleagues Mr. Walter de Vries and Mr. Bas Bruins Slot, whose supports for carrying out the numerical experiments saved me a lot of computational time.

Last but not least, the encouragements and supports from my family and friends are highly appreciated.

Zhiwei Qian

Delft, April 2008

Table of Contents

Chapter 1 Introduction

1.1 Motivation

In the field of material science, one aim is to understand materials fundamentally so that new materials with the desired properties can be created.

The objective of this MSc thesis project is to establish a numerical model that helps scientists and engineers to look into a kind of interesting material: cement paste.

Portland cement is a fundamental material for civil engineering structures and has some unique properties. First of all, the state of cement changes once it is mixed with water, this phenomenon is called hydration reaction, and the final product is named cement paste. With the increasing of degree of hydration, the properties of cement paste are changing all the time, among other things, two of which are the tensile strength and stiffness. Furthermore, cracking is another characteristic of cement paste, which is primarily due to the limited capacity to sustain tensile stresses (or perhaps better, tensile strains) [1].

This project studies the fracture process of cement paste, especially the tensile strength, stiffness and cracking due to external loads. Moreover, the study is based on the micro-structure of cement paste at the level of micro-meter so that the relationship between micro-structure of materials and the corresponding properties is revealed.

1.2 Similar efforts

Numerical modeling of fracture process of brittle materials, such as cement paste, mortar, concrete and rocks, started in the late 1960s with the landmark papers of Ngo and Scordelis (1967) [2] and Rashid (1968) [3], in which the discrete and smeared crack models were introduced. Especially the latter approach gained much popularity, and in the 1970s comprehensive efforts were invested in developing constitutive models in a smeared setting which could reproduce the experimentally observed stress-strain characteristics of concrete. However, they cannot tell the fracture process in detail. [4]

In the 1990s, Schlangen and van Mier proposed another model to compensate the drawbacks of discrete and smeared crack models, which is called lattice model [5]. The concept “Lattice” was borrowed from the filed of theoretical physics and was first introduced to material science by Hrennikoff in the 1940s [6]. In the lattice model, the continuum is replaced by a lattice of truss or beam elements. Subsequently, the micro-structure of the material can be mapped onto these truss or beam elements by assigning them different properties, depending whether the truss or beam element represents a grain or mortar. However, the research was mainly in the 2D domain.

Up to the year 2007, all these studies were at the meso-level, hence, they could not illustrate a direct relationship between the micro-structure of materials and the corresponding performance. In 2007, Tan tried to link the existing hydration model HYMOSTRUC (Hydration, Morphology and Structure) [7, 8] and the lattice fracture model. She lay down several assumptions to generate an irregular lattice mesh on basis of the micro-structure information provided by the hydration model HYMOSTRUC. She primarily studied the problem in 2D domain and took an attempt for 3D analysis. One of her conclusions was “The numerical results from 2D and 3D lattice models differ a lot. It is suggested to apply 3D lattice model for further numerical research.” [9]

1.3 Objective

In this project, a complete 3D analysis of cement paste is done, more specifically, two modules, namely 3D Lattice Generation and 3D Lattice Analysis, are developed. The first module can be regarded as an upgrade of Tan's work, as some assumptions related to the lattice mesh are improved. The latter one, 3D Lattice Analysis, is an extension of Schlangen's program to 3D domain. The differences and improvements of modeling in this thesis compared with existing works [5, 9] are briefly described in Chapter 2.

1.4 Overview

According to Finite Element Method, the entire analysis can be divided into three stages: pre-processing, kernel and post-processing. In this project, pre-processing is the 3D Lattice Generation, then is the kernel 3D Lattice Analysis, the last phase is to interpret the results from 3D Lattice Analysis, for instance, visualization of load-displacement diagram and crack propagation.

The starting point of this research is the outcome from HYMOSTRUC model, which illustrates the micro-structure information of cement paste. The final output of this project is the load-displacement diagram and the crack propagation. Figure 1.1 shows the complete procedures.

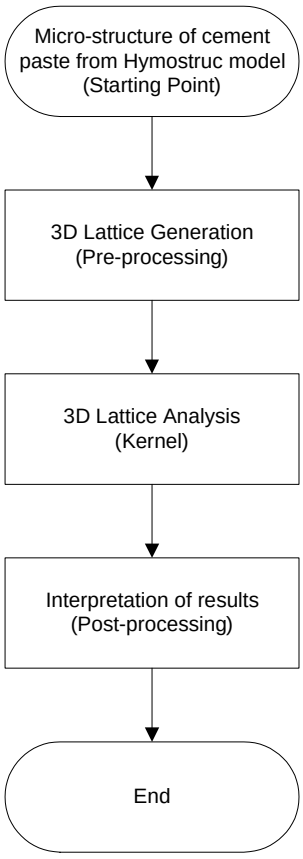

Figure 1.1 Flow chart of the project

1.5 Outline of the thesis

The thesis is divided into seven chapters.

Chapter 1 introduces the motivation of this research and reviews similar efforts in literatures. The objective and overview of this thesis are also presented.

Chapter 2 illustrates the differences and improvements of modeling in this thesis compared with existing works.

Chapter 3 creates the numerical model of cement paste, including all the stages shown in Figure 1.1.

Chapter 4 determines the basic parameters which are introduced in the numerical model in the preceding chapter.

Chapter 5 presents an example of numerical simulation, which follows the entire procedures defined in Chapter 3 and uses the basic parameters determined in Chapter 4.

Chapter 6 gives and compares the results (e.g. tensile strength and stiffness) of a set of numerical simulations, mainly concerning the variation of curing ages and Blaine values.

Chapter 7 summarizes the main contribution of this thesis, points out the limitations of current model and implementation, and proposes suggestions for further investigation.

Chapter 2 Modeling Review

This chapter intends to briefly illustrate the differences and improvements of this thesis compared with the methods adopted in [5] and [9].

2.1 Lattice generation

The mesh method proposed in this thesis is similar to the method adopted in [9]. The differences lie in two aspects, namely the determination of radius of cross-section of local element and the determination of Young's and shear modulus of local element (see Section 3.2 for more information).

In [9], the radius of cross-section of local element is calculated on basis of the volumes of the two contact particles, while in this thesis it is determined by the contact volume of the two contact particles. This approach is based on the assumption "The strength of two contact particles is determined by the weakest link, not the average capacity". Hence, the resulting radius is always smaller than the one in [9].

For the determination of Young's and shear modulus of element, [9] first classifies various contact cases and then calculates the weighted average value directly. In contrast, they are calculated via two "averaging" steps in this research. The advantage of this improvement is that it can avoid complicated classification of contact cases and analytical comparison shows that the result does not differ too much.

2.2 Lattice analysis

In [5], the concept "Lattice" was first introduced into the field of fracture mechanics and a new cracking model was proposed, namely lattice fracture model. However, it was restricted to 2D analysis of concrete at meso-level, although the principles also hold for other configurations. This thesis expands the implementation to 3D analysis and at a lower level (micro-level) for cement paste (see Section 3.3 for more information). Furthermore, the burning algorithm is incorporated to determine when to stop the analysis. This change is necessary for random geometric lattice, and the reason is illustrated in Section 3.3.12.

Chapter 3 Numerical Modeling

This chapter is the spirit of the thesis project, as it establishes the modeling approach.

3.1 Starting point

The starting point of this research is the micro-structure information which comes from the hydration model HYMOSTRUC. In this model, it is assumed that only CSH (Calcium Silicate Hydrates) and CH (Calcium Hydroxides) are produced during the hydration process. From fracture point of view, there is not too much difference between the hydration product CSH and CH, hence, CH product is transferred to volume equivalent CSH product for simplicity in this research. The outcome object is assumed to be in the shape of sphere and consist of three layers in general, namely unhydrated cement, inner product and outer product. The location of the object is expressed by sphere center coordinates and the size by diameters. This object is named as hydrating cement particle for convenient reference.

The output file from the program HYMOSTRUC has the extension *.hym, the syntax of which looks like

Table 3.1 *.hym (HYMOSTRUC)

x	y	z	D_outer	type	D_inner	D_unhydrated
…	…	…	…	…	…	…

3.2 3D Lattice Generation

The reason for defining this step is that the outcome from HYMOSTRUC model is not exactly what is required by lattice model. The lattice analysis operates on a frame structure while the HYMOSTRUC model only provides the micro-structure information in terms of spheres. Hence, additional operation is demanded to generate a frame structure consisting of beam elements on basis of the output from HYMOSTRUC. Fortunately, it is not difficult to build this bridge, which will be elaborated in the following sections.

3.2.1 Required parameters

In the lattice analysis module, it is assumed that the frame consists of beam elements with circular cross-section. Hence, the task of lattice generation is to determine the location of nodes, the geometric parameters (e.g. length, radius of cross-section) and mechanical properties (e.g. Young's and shear modulus, tensile strength) of elements.

3.2.2 Determination of nodes and geometric parameters

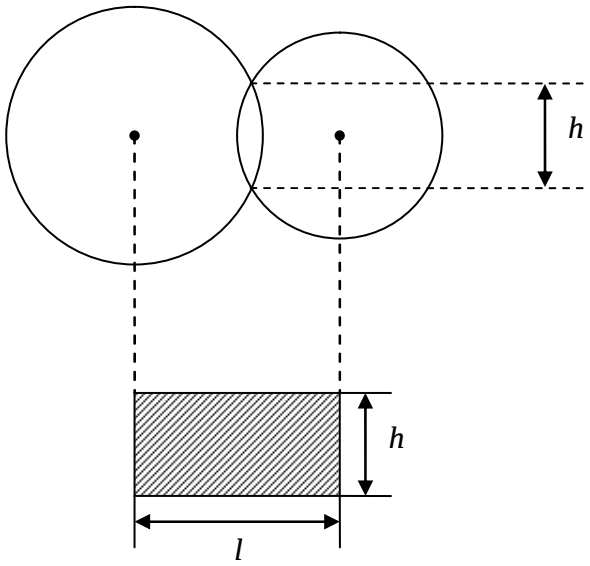

Figure 3.1 Contact hydrating cement particles and beam element

It is reasonable to assume that one node represents one hydrating cement particle, hence, the node coordinates are exactly equal to the coordinates of hydrating cement particle center. Moreover, it is assumed that one element is generated between two hydrating cement particles if they have contact volume as shown in Figure 3.1. The length of the element is equal to the distance of the two nodes, the radius of cross-section is determined by the size of contact volume.

3.2.3 Determination of Young's and shear modulus of element

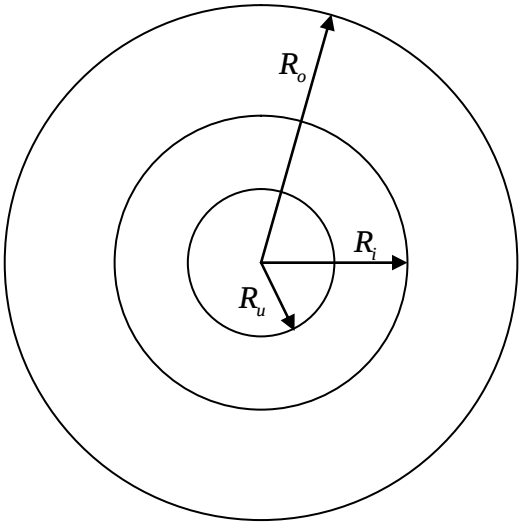

$$E_p = \frac{R_u}{R_o} E_u + \frac{R_i - R_u}{R_o} E_i + \frac{R_o - R_i}{R_o} E_o$$

where,

E_p = modulus of particle
E_u = modulus of unhydrated cement
E_i = modulus of inner product
E_o = modulus of outer product
R_u = radius of unhydrated cement
R_i = radius of inner product
R_o = radius of outer product

Figure 3.2(a) Determination of particle modulus

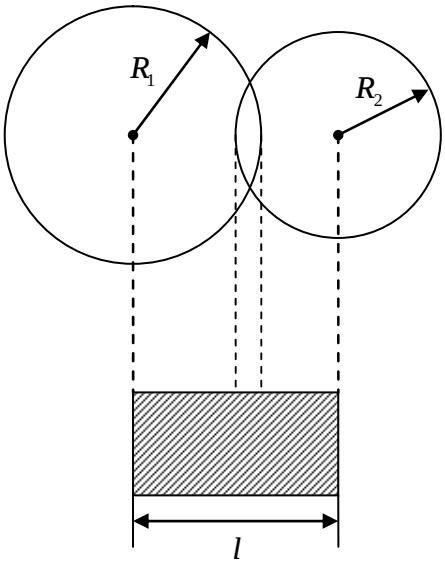

$$E = \frac{l - R_2}{l} E_{p1} + \frac{R_1 + R_2 - l}{l} \frac{E_{p1} + E_{p2}}{2} + \frac{l - R_1}{l} E_{p2}$$

where,

E = modulus of beam element

E_{p1} = modulus of particle 1

E_{p2} = modulus of particle 2

R_1 = radius of particle 1

R_2 = radius of particle 2

l = length of beam element

Figure 3.2(b) Determination of beam element modulus

For the determination of Young's and shear modulus of element (E, G), it is not so straightforward. In this research, they are calculated via two "averaging" steps as shown in Figure 3.2(a) and (b). First of all, the modulus of hydrating cement particle (E_p, G_p) is defined as average value of modulus of unhydrated cement, inner product and outer product by weight. Then modulus of element can be calculated by averaging particle modulus by weight.

3.2.4 Determination of tensile strength of element

The last parameter to be determined is the tensile strength of element. Actually this is the trickiest one in the lattice model. For simplicity, it is assumed that the tensile strength is proportional to the Young's modulus of the element. The coefficient is determined in Section 4.3.

3.3 3D Lattice Analysis

The role of lattice analysis in this research is to simulate the fracture process of cement paste system. The basic idea of lattice analysis is that imposing a prescribed displacement on a frame structure, finding the critical element that has highest stress/strength ratio, removing it from the system. This procedure is repeated until the system fails.

Roughly speaking, lattice analysis is a set of linear analysis on frame structures using Finite Element Method. This implies that the fundamental of lattice analysis is nothing else but the conventional structural analysis. As a result, the steps required for lattice analysis are quite similar to the standard finite element analysis for space frame structure, except that the critical element is removed and the analysis is repeated until the system fails. It is illustrated by Figure 3.3.

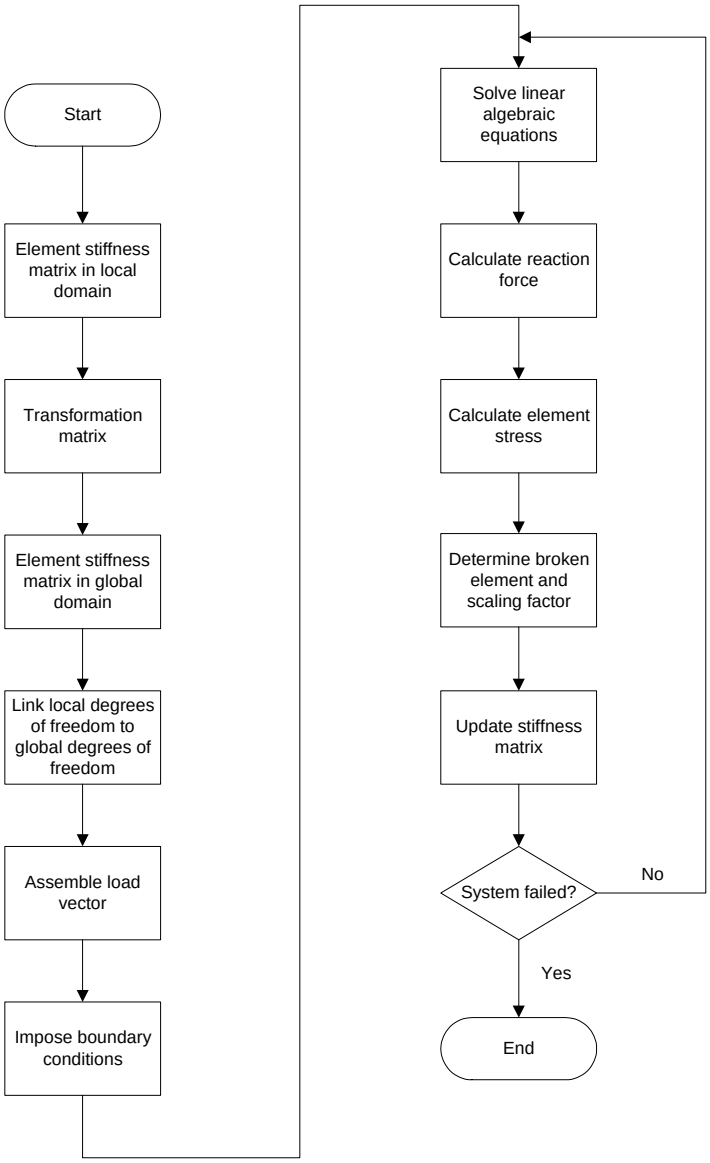

Figure 3.3 Lattice analysis flow chart

3.3.1 Element stiffness matrix in local domain

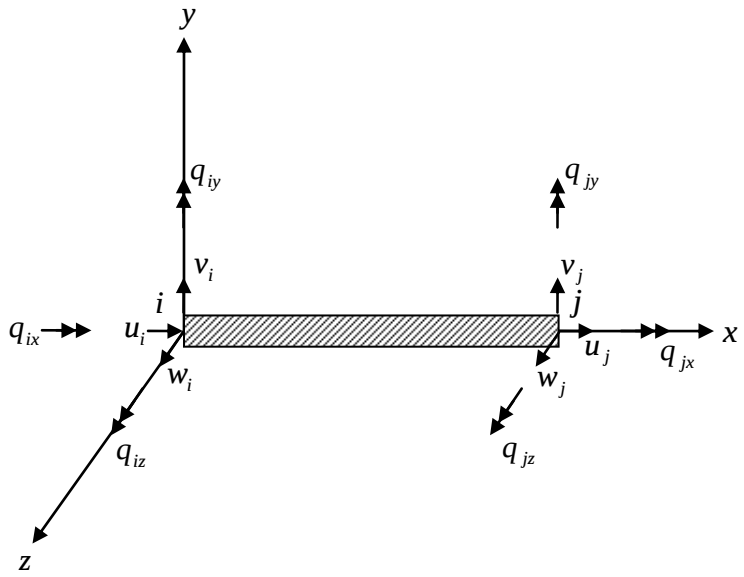

Figure 3.4 Local domain

In this research, the two-noded beam element in 3D configuration is adopted as shown in Figure 3.4. Shear effect is taken into account because both slender and non-slender elements are presented for the mesh generated in Section 3.2.

The complete form of element stiffness matrix is in the dimension of 12×12, which consists of the following contributions,

(1) For axial deformation,

$$\underline{\underline{K}}^{e}_{(1)} = \begin{bmatrix} \frac{EA}{l} & -\frac{EA}{l} \\ sym. & \frac{EA}{l} \end{bmatrix}$$

(2) For bending and shear deformation in the plane xoy,

$$\underline{\underline{K}}^{e}_{(2)} = \begin{bmatrix} \frac{12EI_z}{l^3(1+\Phi_1)} & \frac{6EI_z}{l^2(1+\Phi_1)} & -\frac{12EI_z}{l^3(1+\Phi_1)} & \frac{6EI_z}{l^2(1+\Phi_1)} \\ & \frac{(4+\Phi_1)EI_z}{l(1+\Phi_1)} & -\frac{6EI_z}{l^2(1+\Phi_1)} & \frac{(2-\Phi_1)EI_z}{l(1+\Phi_1)} \\ & & \frac{12EI_z}{l^3(1+\Phi_1)} & -\frac{6EI_z}{l^2(1+\Phi_1)} \\ sym. & & & \frac{(4+\Phi_1)EI_z}{l(1+\Phi_1)} \end{bmatrix}$$

(3) For bending and shear deformation in the plane *xoz* ,

$$\underline{\underline{K}}^{e}_{(3)} = \begin{bmatrix} \frac{12EI_y}{l^3(1+\Phi_2)} & -\frac{6EI_y}{l^2(1+\Phi_2)} & -\frac{12EI_y}{l^3(1+\Phi_2)} & -\frac{6EI_y}{l^2(1+\Phi_2)} \\ & \frac{(4+\Phi_2)EI_y}{l(1+\Phi_2)} & \frac{6EI_y}{l^2(1+\Phi_2)} & \frac{(2-\Phi_2)EI_y}{l(1+\Phi_2)} \\ & & \frac{12EI_y}{l^3(1+\Phi_2)} & \frac{6EI_y}{l^2(1+\Phi_2)} \\ \textit{sym.} & & & \frac{(4+\Phi_2)EI_y}{l(1+\Phi_2)} \end{bmatrix}$$

(4) For torsion,

$$\underline{\underline{K}}^{e}_{(4)} = \begin{bmatrix} \frac{GJ}{l} & -\frac{GJ}{l} \\ \textit{sym.} & \frac{GJ}{l} \end{bmatrix}$$

The element stiffness matrix can be assembled on basis of the above four components, which is

$$\underline{\underline{K}}^{e} = \begin{bmatrix} \frac{EA}{l} & 0 & 0 & 0 & 0 & 0 & -\frac{EA}{l} & 0 & 0 & 0 & 0 & 0 \\ & \frac{12EI_z}{l^3(1+\Phi_1)} & 0 & 0 & 0 & \frac{6EI_z}{l^2(1+\Phi_1)} & 0 & -\frac{12EI_z}{l^3(1+\Phi_1)} & 0 & 0 & 0 & \frac{6EI_z}{l^2(1+\Phi_1)} \\ & & \frac{12EI_y}{l^3(1+\Phi_2)} & 0 & -\frac{6EI_y}{l^2(1+\Phi_2)} & 0 & 0 & 0 & -\frac{12EI_y}{l^3(1+\Phi_2)} & 0 & -\frac{6EI_y}{l^2(1+\Phi_2)} & 0 \\ & & & \frac{GJ}{l} & 0 & 0 & 0 & 0 & 0 & -\frac{GJ}{l} & 0 & 0 \\ & & & & \frac{(4+\Phi_2)EI_y}{l(1+\Phi_2)} & 0 & 0 & 0 & \frac{6EI_y}{l^2(1+\Phi_2)} & 0 & \frac{(2-\Phi_2)EI_y}{l(1+\Phi_2)} & 0 \\ & & & & & \frac{(4+\Phi_1)EI_z}{l(1+\Phi_1)} & 0 & -\frac{6EI_z}{l^2(1+\Phi_1)} & 0 & 0 & 0 & \frac{(2-\Phi_1)EI_z}{l(1+\Phi_1)} \\ & & & & & & \frac{EA}{l} & 0 & 0 & 0 & 0 & 0 \\ & & & & & & & \frac{12EI_z}{l^3(1+\Phi_1)} & 0 & 0 & 0 & -\frac{6EI_z}{l^2(1+\Phi_1)} \\ & & & \textit{sym.} & & & & & \frac{12EI_y}{l^3(1+\Phi_2)} & 0 & \frac{6EI_y}{l^2(1+\Phi_2)} & 0 \\ & & & & & & & & & \frac{GJ}{l} & 0 & 0 \\ & & & & & & & & & & \frac{(4+\Phi_2)EI_y}{l(1+\Phi_2)} & 0 \\ & & & & & & & & & & & \frac{(4+\Phi_1)EI_z}{l(1+\Phi_1)} \end{bmatrix}$$

where,

$$\Phi_1 = \frac{12EI_z}{GA_s l^2}$$

$$\Phi_2 = \frac{12EI_y}{GA_s l^2}$$

$$A_s = \frac{A}{k}$$

E = Young's modulus

G = shear modulus
I_z = moment of inertial about z-axis
I_y = moment of inertial about y-axis
J = polar moment of inertial about x-axis
A = cross-sectional area
A_s = shear cross-sectional area
k = shear correction factor

In particular, for circular cross-section,

$$I_z = \frac{p}{4} r^4$$

$$I_y = \frac{p}{4} r^4$$

$$J = \frac{p}{2} r^4$$

$$A = p r^2$$

$$k = \frac{10}{9}$$

3.3.2 Transformation matrix

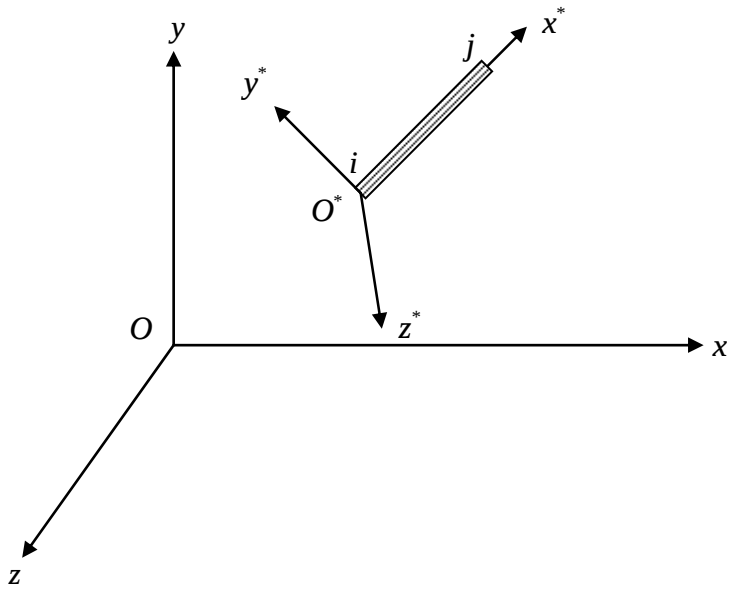

Figure 3.5 Local and global coordinate systems

The configuration of 3D beam element is shown in Figure 3.5. The transformation matrix is of the following form,

$$\underline{\underline{T}} = \begin{bmatrix} \underline{t} & & & \\ & \underline{t} & & \\ & & \underline{t} & \\ & & & \underline{t} \end{bmatrix}$$

where,

$$\underline{t} = \begin{bmatrix} l_1 & l_2 & l_3 \\ m_1 & m_2 & m_3 \\ n_1 & n_2 & n_3 \end{bmatrix}$$

Direction cosines are

$l_1 = \cos(x, x^*)$

$l_2 = \cos(x, y^*)$

$l_3 = \cos(x, z^*)$

$m_1 = \cos(y, x^*)$

$m_2 = \cos(y, y^*)$

$m_3 = \cos(y, z^*)$

$n_1 = \cos(z, x^*)$

$n_2 = \cos(z, y^*)$

$n_3 = \cos(z, z^*)$

These nine direction cosines can be determined on basis of the coordinates of the two nodes $i(x_i, y_i, z_i)$ and $j(x_j, y_j, z_j)$ in global domain. The procedure is

(1) $a_1 = x_j - x_i$

$a_2 = y_j - y_i$

$a_3 = z_j - z_i$

(2) choose an arbitrary reference point $B(x_b, y_b, z_b)$ on the principal plane $x^*O^*y^*$ or $x^*O^*z^*$, provided that the point B is not located on the x^*-axis

$b_1 = x_b - x_i$

$b_2 = y_b - y_i$

$b_3 = z_b - z_i$

(3) $c_1 = a_2 b_3 - a_3 b_2$

$c_2 = a_3 b_1 - a_1 b_3$

$c_3 = a_1 b_2 - a_2 b_1$

(4) $d_1 = c_2 a_3 - c_3 a_2$

$d_2 = c_3 a_1 - c_1 a_3$

$d_3 = c_1 a_2 - c_2 a_1$

(5) $l = \sqrt{a_1{}^2 + a_2{}^2 + a_3{}^2}$ (length of element)

$$l_1 = \frac{a_1}{l}$$

$$m_1 = \frac{a_2}{l}$$

$$n_1 = \frac{a_3}{l}$$

(6) $d = \sqrt{d_1{}^2 + d_2{}^2 + d_3{}^2}$

$$l_2 = \frac{d_1}{d}$$

$$m_2 = \frac{d_2}{d}$$

$$n_2 = \frac{d_3}{d}$$

(7) $l_3 = m_1 n_2 - m_2 n_1$

$m_3 = n_1 l_2 - n_2 l_1$

$n_3 = l_1 m_2 - l_2 m_1$

3.3.3 Element stiffness matrix in global domain

The element stiffness matrix in global domain $\underline{\underline{K}}^e_{global}$ can be calculated on basis of element stiffness matrix in local domain $\underline{\underline{K}}^e_{local}$ and transformation matrix $\underline{\underline{T}}$ using the formula

$$\underline{\underline{K}}^e_{global} = \underline{\underline{T}}\,\underline{\underline{K}}^e_{local}\,\underline{\underline{T}}^T$$

The resulting matrix is in the dimension of 12×12.

3.3.4 Link local degrees of freedom to global degrees of freedom

The connectivity array is defined to describe the relationship between elements. Local degrees of freedom for an element start from 1 and end at 12, while global degrees of freedom are dependent on the number of nodes in the system and how many degrees of freedom each node has. For beam element in 3D configuration, each node always has six degrees of freedom in global domain, hence the total number of degrees of freedom of the system is $6N$, where N is the number of nodes in the system.

The connectivity array for an element has 12 entries, which can be calculated by

$ConnectivityArray[1] = 6 \times (i-1) + 1$

$ConnectivityArray[2] = 6 \times (i-1) + 2$

$ConnectivityArray[3] = 6 \times (i-1) + 3$

$ConnectivityArray[4] = 6 \times (i-1) + 4$

$ConnectivityArray[5] = 6\times(i-1)+5$
$ConnectivityArray[6] = 6\times(i-1)+6$
$ConnectivityArray[7] = 6\times(j-1)+1$
$ConnectivityArray[8] = 6\times(j-1)+2$
$ConnectivityArray[9] = 6\times(j-1)+3$
$ConnectivityArray[10] = 6\times(j-1)+4$
$ConnectivityArray[11] = 6\times(j-1)+5$
$ConnectivityArray[12] = 6\times(j-1)+6$

where,

i, j are the node number of the first node and second node of an element, respectively

3.3.5 Assemble load vector

The load vector represents all the loads on the system. Please be aware that prescribed displacements are regarded as a kind of displacement boundary conditions (Dirichlet boundaries), not active external loads. As only prescribed displacements are imposed on the system in this research, the resulting load vector is zero-vector.

3.3.6 Impose boundary conditions

In conventional structural analysis, it is time to assemble global stiffness matrix based on the element stiffness matrix in global domain and connectivity array. However, in lattice analysis, the problem size is usually quite huge (for instance, the system consists of 1 million nodes), hence, it is impossible to store such a huge global stiffness matrix in computer memory in practice. The solution is to make use of global stiffness matrix in unassembled form. The corresponding method is usually called element-by-element scheme.

The global stiffness matrix is not assembled, but the information on how it would be assembled can be gathered from element stiffness matrix in global domain and connectivity array. For convenient reference, the phrase "global stiffness matrix" mentioned in this thesis means element stiffness matrix in global domain plus connectivity array.

The prescribed displacement boundary conditions can be imposed element-by-element according to the following procedures,

$\underline{\underline{K}}\,\underline{d} \xrightarrow{yields} \underline{f}$

where,

$\underline{\underline{K}}$ is the global stiffness matrix before boundary conditions imposed, which is singular;

$\underline{d}$ is the displacement vector, in which only the constraint entries are known;

$\underline{f}$ is the external load vector, in our particular case it is zero vector as there is no active external loads.

(Remark: Please note that the following procedures also hold even if active external loads exist.)

(1) Fill the unknown entries in the displacement vector $\underline{d}$ with artificial "0";
(2) Calculate the multiplication of global stiffness matrix $\underline{\underline{K}}$ with the displacement vector $\underline{d}$, the result vector is denoted as Δf;
(3) Update the load vector $\underline{f}$ using the formula $f \Leftarrow f - \Delta f$ (Be aware that here is "minus" sign NOT "plus");
(4) Update the constraint entries in the load vector $\underline{f}$ with the product of prescribed displacement multiplied by the corresponding diagonal entry in the global stiffness matrix $\underline{\underline{K}}$;
(5) Set all the entries in the constraint rows and columns in the global stiffness matrix $\underline{\underline{K}}$ to "0", except that the diagonal entry remains.

When the above steps are complete, the prescribed boundary conditions have already been imposed, and the global stiffness matrix $\underline{\underline{K}}$ is not singular any longer.

In order to present the above procedures more straightforward, an example is given as following.

$$\begin{bmatrix} k_{11} & 0 & k_{13} & k_{14} & 0 \\ 0 & k_{22} & 0 & 0 & 0 \\ k_{31} & 0 & k_{33} & k_{34} & 0 \\ k_{41} & 0 & k_{43} & k_{44} & 0 \\ 0 & 0 & 0 & 0 & k_{55} \end{bmatrix} \begin{Bmatrix} 0 \\ c_1 \\ 0 \\ 0 \\ c_2 \end{Bmatrix} \rightarrow \begin{Bmatrix} 0-(c_1 k_{12} + c_2 k_{15}) \\ c_1 k_{22} \\ 0-(c_1 k_{32} + c_2 k_{35}) \\ 0-(c_1 k_{42} + c_2 k_{45}) \\ c_2 k_{55} \end{Bmatrix}$$

where,
c_1 and c_2 are prescribed displacements at the second and fifth degrees of freedom

3.3.7 Solve linear algebraic equations

The global stiffness matrix $\underline{\underline{K}}$ and the load vector $\underline{f}$ turn into the coefficient matrix and constant vector in linear algebraic equations after imposing boundary conditions.

Actually, solving the system of linear algebraic equations is the most time consuming part in the entire analysis. Hence, it is important to choose an appropriate solver and optimize it to satisfy with the specific problem.

After reading some literatures [10], it is decided to apply conjugate gradient iterative method to solve this system of equations because it is suitable for large-scale sparse linear system. Moreover, preconditioning technique is incorporated primarily due to the following two reasons,

(1) The global stiffness matrix $\underline{\underline{K}}$ is probably ill-conditioned due to the irregular mesh constructed in Section 3.2 and preconditioning technique might make the convergence faster even if the coefficient matrix is not well-conditioned;
(2) "It is generally accepted that for large-scale applications, CG (conjugate gradient) should nearly always be used with a preconditioner" [10].

In this project, Jacobi preconditioner is adopted as it is suitable for element-by-element scheme [11].

The basic algorithm for Jacobi-preconditioned conjugate gradient method is presented as following,

Suppose that a system of linear equations is represented by
$Ax = b$
where,
A is the coefficient matrix,
b is the constant vector,
x is the solution vector

Given the inputs A, b, an initial guess x, absolute error tolerance $e_{absolute} < 1$, relative error tolerance $e_{relative} < 1$, and a maximum number of iterations $i_{\max}$. [10]

$m \Leftarrow diag(A)$
$m \Leftarrow m^{-1}$
$r \Leftarrow b - Ax$
$d \Leftarrow m * r$
$d_{new} \Leftarrow r^T d$
$d_0 \Leftarrow d_{new}$
if $d_0 < e^2_{absolute}$, then terminate;
for(unsigned long int $i = 1; i <= i_{\max}; i++$)
{
$q \Leftarrow Ad$
$a \Leftarrow \frac{d_{new}}{d^T q}$
$x \Leftarrow x + a\,d$
$r \Leftarrow r - a\,q$
$s \Leftarrow m * r$
$d_{old} \Leftarrow d_{new}$
$d_{new} \Leftarrow r^T s$
if $d_{new} < e^2_{absolute}$ or $d_{new} < e^2_{relative} d_0$, then terminate;
$b \Leftarrow \frac{d_{new}}{d_{old}}$
$d \Leftarrow s + b\,d$
}

3.3.8 Calculate reaction force

The reaction force is the summation of node forces of the constraint nodes which are in the same group. Node forces can be calculated using the following formula,

$\underline{f} = \underline{\underline{K}}\underline{d}$

where,

$\underline{f}$ is the node force vector,

$\underline{\underline{K}}$ is the global stiffness matrix before boundary conditions imposed, which is singular,

$\underline{d}$ is the displacement vector, which is the solution from Section 3.3.7

3.3.9 Calculate element stress

The element internal forces can be calculated via two steps, using the formulas

$\underline{d}^e_{local} = \underline{\underline{T}}^T \underline{d}^e_{global}$

$\underline{f}^e_{local} = \underline{\underline{K}}^e_{local} \underline{d}^e_{local}$

where,

$\underline{\underline{T}}$ is the transformation matrix of an element,

$\underline{\underline{K}}^e_{local}$ is the element stiffness matrix in local domain,

$\underline{d}^e_{global}$ is the element displacement vector in global domain,

$\underline{d}^e_{local}$ is the element displacement vector in local domain,

$\underline{f}^e_{local}$ is the element internal force vector in local domain

Various element stresses can be calculated based on the element internal forces. In this research, the comparative element stress is defined as

$$s_{comparative} = \frac{N}{A}$$

where,

N is the element normal force, "+" represents tension while "−" compression,

A is the area of an element

3.3.10 Determine broken element and scaling factor

At this step, the stress/strength ratio is calculated for every element and the element which has highest stress/strength ratio is defined as critical element. The critical element will be removed from the system and never comes back again. Furthermore, this removed element represents a void in the material, thus an alternative name for critical element is "broken element".

The inverse of the highest stress/strength ratio is defined as scaling factor. As the imposed prescribed displacement does not change during the entire analysis, this factor is used to derive the actual deformation of the system to reach the critical state.

3.3.11 Update stiffness matrix

The method to remove an element from the system is to update the corresponding stiffness matrices. The element stiffness matrices in local and global domain are cleared by setting all entries to zero and its contribution to the global stiffness matrix is eliminated. In such a way, the system is weakened.

3.3.12 Check failure of the system

In principle, the reaction force is going to zero when the system fails. However, this case seldom takes place due to numerical errors in practice. Generally speaking, setting an error tolerance would be a solution, but unfortunately it is not reasonable for the lattice analysis because it is difficult to predict the lower bound of reaction forces which can be very small or extremely large.

In this study, the problem is solved by checking the connectivity of remaining lattice structure. From physical point of view, if there is no path which links the top layer of the specimen to the bottom layer in the case of tension test in vertical direction, then the system fails. Hence, checking the connectivity of the lattice system is a straightforward way to determine whether the analysis should be stopped. In this research, burning algorithm is adopted to check the connectivity of the lattice system. More specifically, the boundary nodes are chosen as starting nodes, and then looking for and burning their neighbors. The burned neighbor nodes are chosen as new starting nodes. The above procedures are carried out recursively until no more nodes can be burned.

3.4 Interpretation of results

During the lattice analysis, the reaction force, broken element number and scaling factor are recorded. The derived results can be sorted into two catalogues for different usage, one is for simulation of mechanical properties and the other is for prediction of crack propagation.

The mechanical properties is given in terms of load-displacement diagram, while the crack propagation is described by two different methods, namely element based method and voxel based method.

In element based method, one broken element represents one micro-crack in the material. The elongation of broken element is defined as micro-crack width in 2D configuration. In 3D configuration, the micro-crack is assumed to be in the shape of cylinder, the length of which is the elongation of broken element and the cross-section of which is equal to the cross-section of broken element. This approach can show the location of micro-cracks and the amount of cracks approximately. However, it cannot provide accurate information for further analysis, for instance, the permeability of the cement paste. Furthermore, it is not flexible because it is not allowed to remove part of the entire broken element.

An alternative is to transfer the broken element to a set of voxels. When an element is removed from the system, the corresponding voxels are removed entirely or partly, the manner of which is specified by the user. As the cracks are described on basis of voxels, it is even possible to add the mico-cracks induced by initial imperfection.

Chapter 4 Determination of Basic Parameters in Model

In Chapter 3, a numerical model is created to analyze the fracture process of cement paste. This chapter will illustrate the involved basic parameters and determine them in detail.

4.1 Basic parameters in the numerical model

In summary, the following parameters must be prepared for the numerical simulation in advance,

(1) Young's modulus and shear modulus of the compounds: unhydrated cement, inner product (high density CSH) and outer product (low density CSH);
(2) The coefficient g which determines the relationship between tensile strength and Young's modulus of local element.

4.2 Young's modulus and shear modulus of the compounds

In this research, the Young's modulus and shear modulus of the compounds which include unhydrated cement, inner product and outer product are taken from [12], which were measured by nano-indentation or mechanical tests as shown in Table 4.1.

Table 4.1 Young's modulus and shear modulus of the compounds in GPa [12]

	Unhydrated cement	Inner product	Outer product
Young's modulus	130	30	22
Shear modulus	50	12.1	8.87

4.3 The coefficient g

Actually, the tensile strength of element is the trickiest parameter in the lattice model. For simplicity, it is assumed that the tensile strength is proportional to the Young's modulus of the element. Then the problem turns to the determination of this proportional coefficient which is denoted by g . In [13], this coefficient is assumed to be 0.0001. In this research, a possible experiment plan is made to get the coefficient g , but it has not been carried out due to lack of appropriate clamp (Currently the Microlab is developing the desired clamp). Hence, the value 0.0001 is used in all the numerical simulations in this thesis.

4.3.1 Experiment plan to determine the coefficient g

The coefficient to be determined shows the relationship between tensile strength and Young's modulus of local element. However, it is difficult to measure it directly because the size of local element is too small (around several micro-meters in this research). The solution is to apply an indirect measurement and derive it based on some assumptions.

The basic idea of the experiment is to measure the tensile strength and Young's modulus of the cubes with different sizes which are large enough to be casted in the lab. For instance, the sizes are varied at $7.5\times7.5\times7.5mm^3$, $15\times15\times15mm^3$ and $22.5\times22.5\times22.5mm^3$. The experiment can be carried out on the micro tension-compression testing device shown in Figure 4.1 with appropriate clamp.

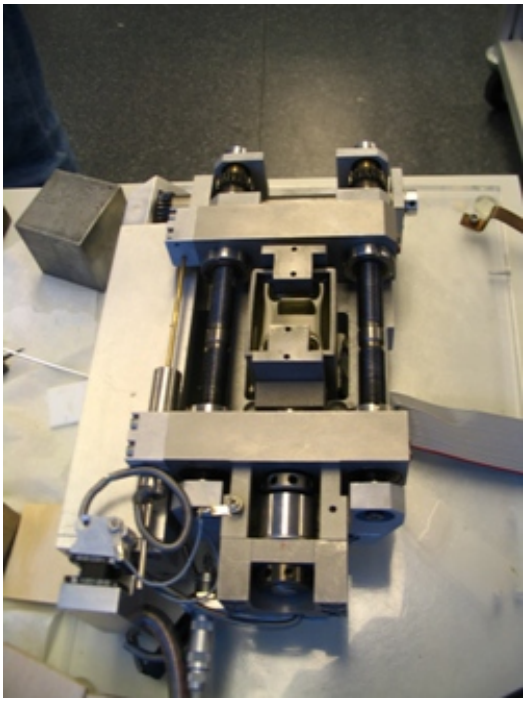

Figure 4.1 Photograph of the micro tension-compression testing device

The experimental results can be summarized in Table 4.2.

Table 4.2 Experimental results

Size	$7.5\times7.5\times7.5mm^3$	$15\times15\times15mm^3$	$22.5\times22.5\times22.5mm^3$
Tensile strength (f_t)	f_{t1}	f_{t2}	f_{t3}
Young's modulus (E)	E_1	E_2	E_3
Coefficient ($g=\frac{f_t}{E}$)	g_1	g_2	g_3

The relationship between the coefficient g and the size of cube can be assumed to be linear, then the coefficient g for the size $1mm$ can be determined on basis of the coefficients g_1, g_2 and g_3.

4.3.2 Influence of the coefficient g

The coefficient g determines the relationship between tensile strength and Young's modulus of local element by $f_t = gE$, while the scaling factor in the lattice model is equal to the inverse of highest stress/strength ratio, which is

$$b=\frac{1}{\frac{s_{comparative}}{f_t}}=\frac{gE}{s_{comparative}}$$

where,

b is the scaling factor,

$s_{comparative}$ is the comparative stress, which is calculated on basis of element stresses,

f_t is the tensile strength of element,

E is the Young's modulus of element

From the above expression, it is obvious that the coefficient g has linear influence on the lattice model, which means it can be used as a fit factor for the final load-displacement diagram.

Chapter 5 An Example of Numerical Simulation

This chapter intends to illustrate an example of numerical simulation using the model created in Chapter 3 and the parameters determined in Chapter 4.

5.1 Simulation of hydration process using HYMOSTRUC

The micro-structure of cement paste can be obtained by the cement hydration and microstructure formation model HYMOSTRUC. In this example, the cement paste is in the shape of cube with the dimension of $100\times100\times100mm^3$. The Blaine value of cement is $420m^2/kg$ and the water/cement ratio is 0.4. The mineralogical composition of the Portland cement used in this study is given in percentage of weight content in Table 5.1.

Table 5.1 Mineralogical composition of the cement CEM I 32.5R [8]

C_3S	C_2S	C_3A	C_4AF
63%	13%	8%	9%

Figure 5.1 illustrates the relationship between the degree of hydration and curing age, which is one of the outcomes from HYMOSTRUC model.

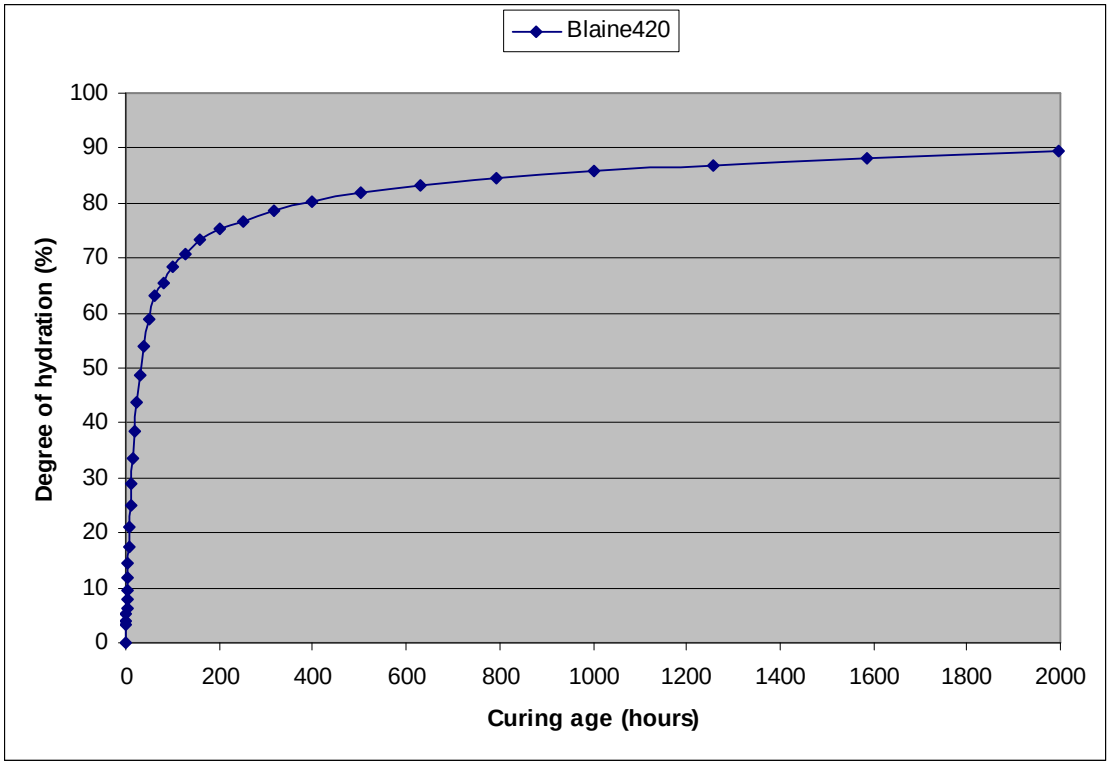

Figure 5.1 Relationship between the degree of hydration and curing age

Figure 5.2 shows an image of the micro-structure of the cement paste at the curing age 794 hours, and the corresponding degree of hydration is 85%.

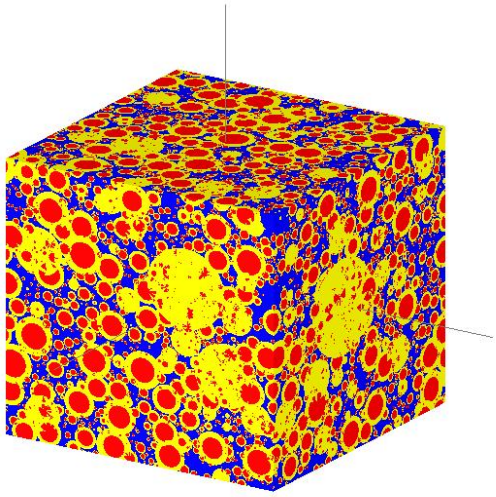

Figure 5.2 Image of cement paste micro-structure (water/cement = 0.4, degree of hydration = 85%)

5.2 3D lattice mesh of the system

Using the method proposed in Section 3.2, a space frame system can be generated on basis of the particle system, which is shown in Figure 5.3. The 3D lattice analysis will operate on this frame system rather than the particle system shown in Figure 5.2.

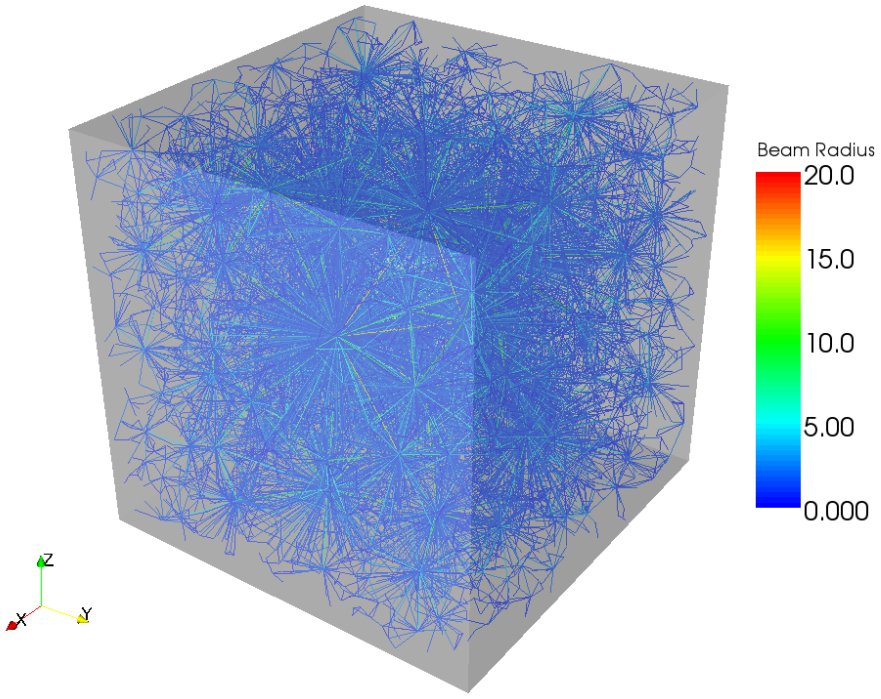

Figure 5.3 3D lattice mesh

5.3 Configuration and results of 3D lattice analysis

In this example, a tension test is carried out on the specimen. The force applied is a uniform surface load in the z-direction, all the other surfaces are free to expand and/or shrink, as shown in Figure 5.4.

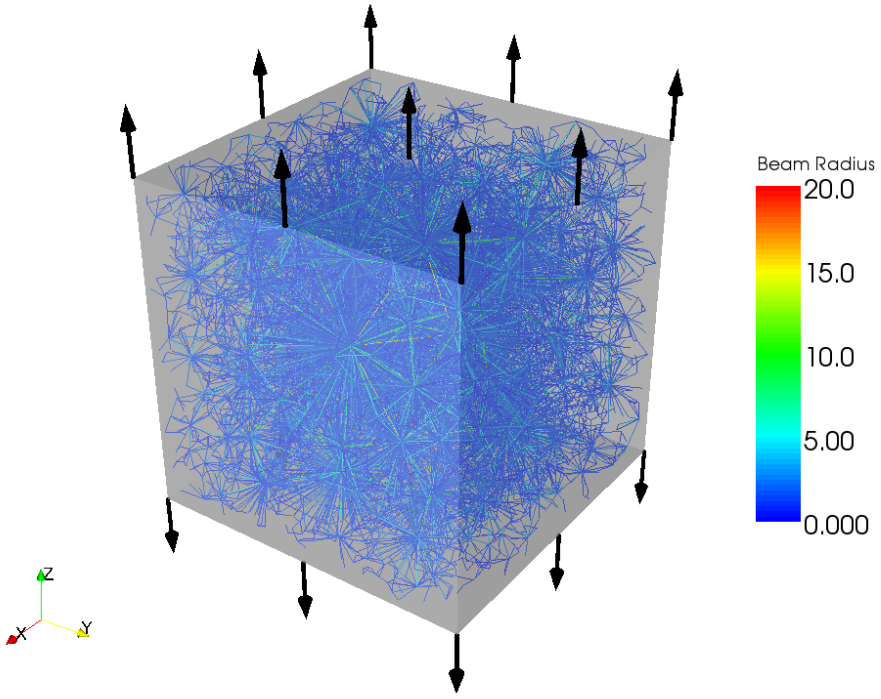

Figure 5.4 Applied load and boundary conditions

In total, 1755 analysis steps are performed until the system fails. The final load-displacement diagram is presented in Figure 5.5. The tensile strength of the cement paste can be obtained, which is $2.14MPa$ and the stiffness (represented by Young's modulus) in the elastic stage can be calculated, which is equal to $1.66\times10^{4}MPa$ (see Section 6.1 and Section 6.2 for more information).

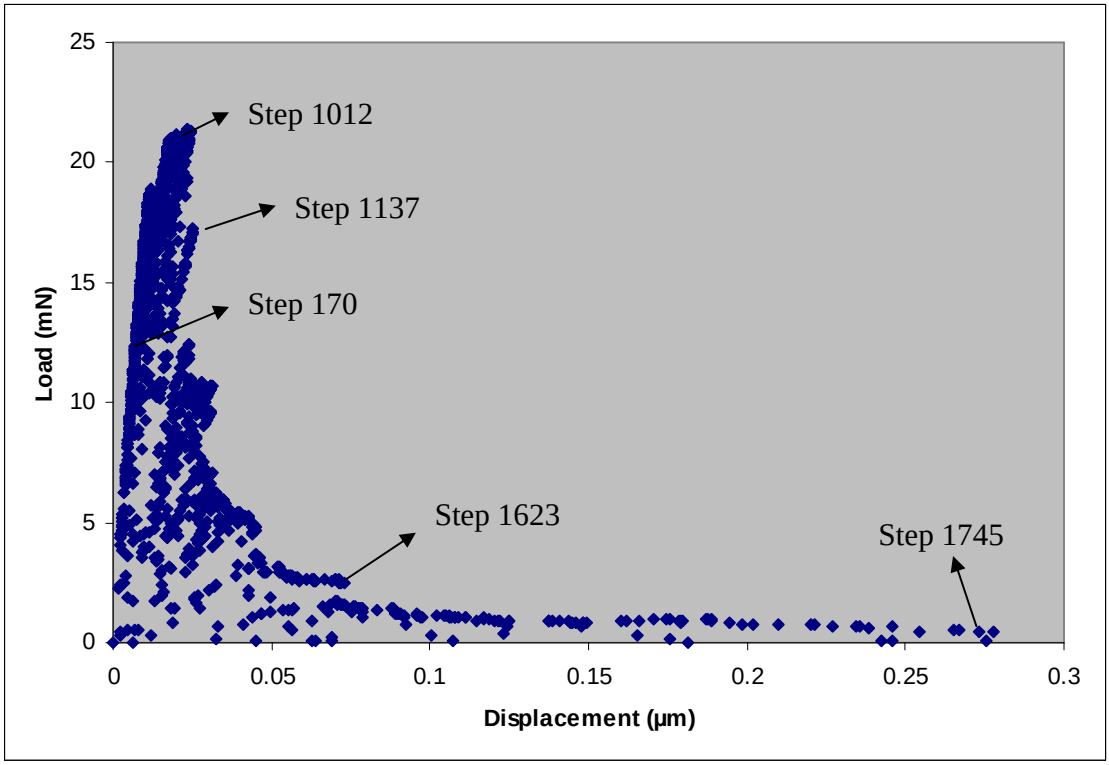

Figure 5.5 Load-displacement diagram

The crack propagation is shown in Figure 5.6(a)~(e) using the element based method proposed in Section 3.4.

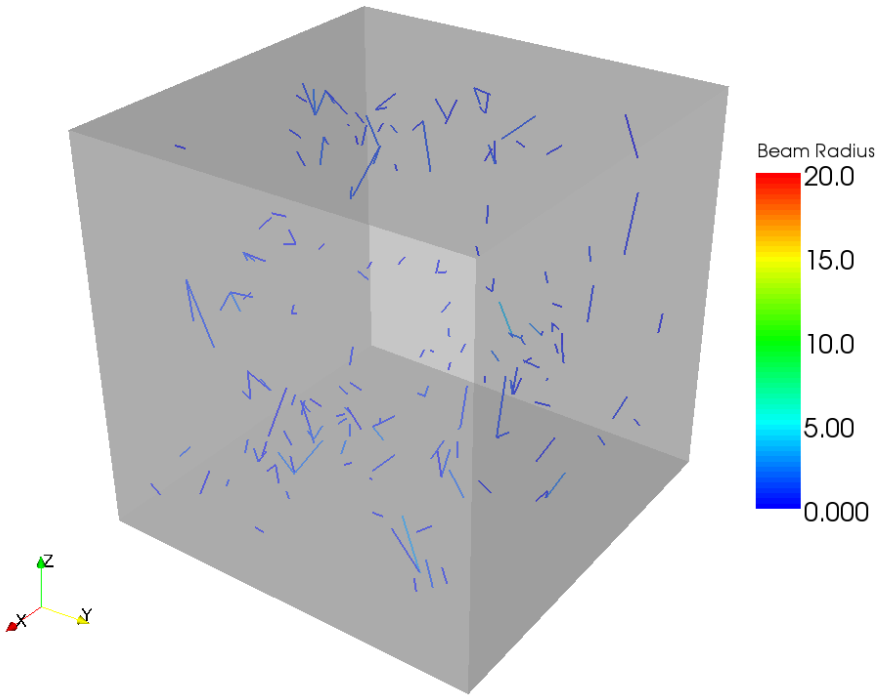

Figure 5.6(a) 3D crack propagation at Step 170

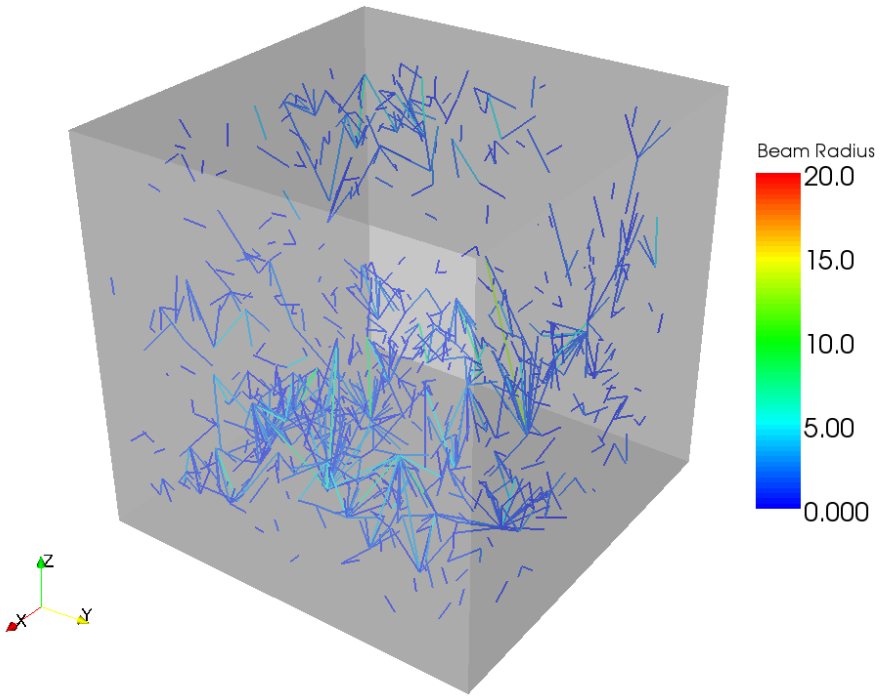

Figure 5.6(b) 3D crack propagation at Step 1012

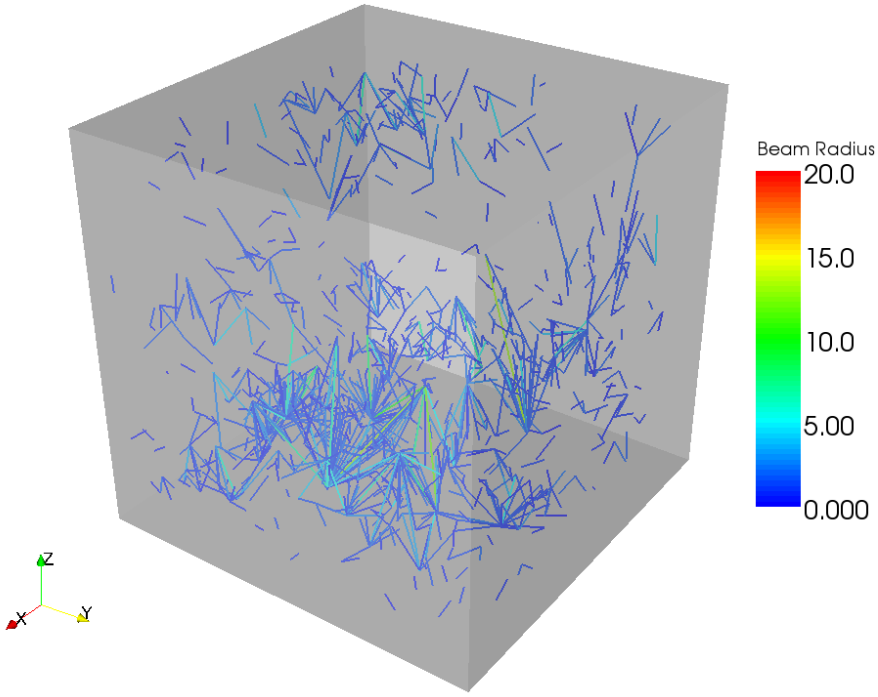

Figure 5.6(c) 3D crack propagation at Step 1137

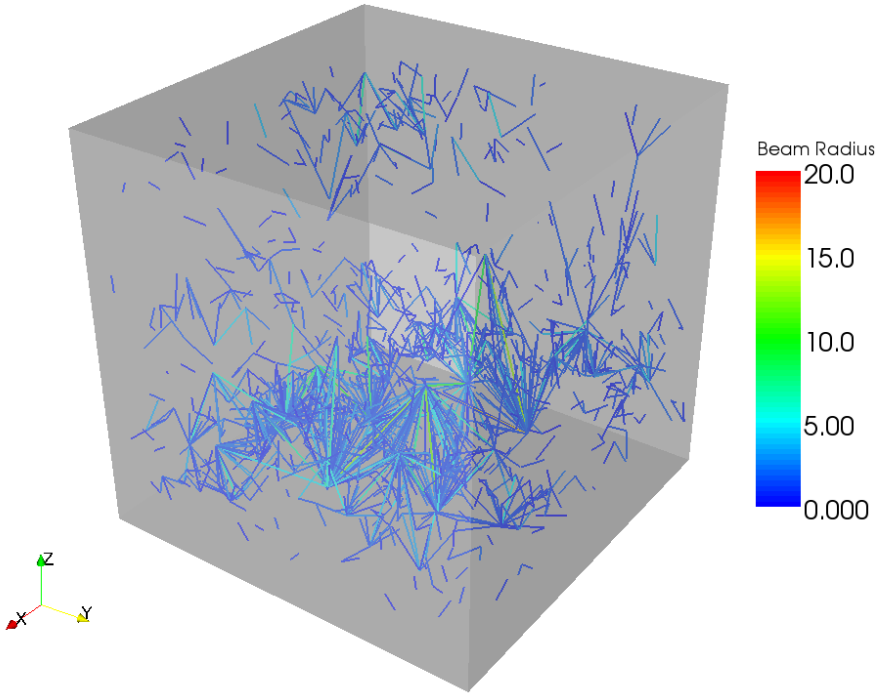

Figure 5.6(d) 3D crack propagation at Step 1623

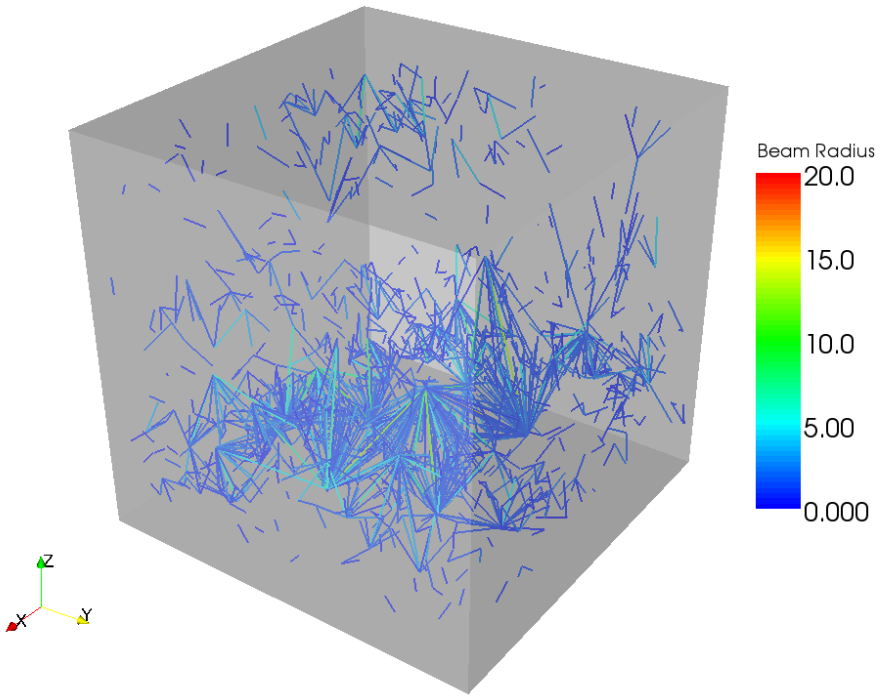

Figure 5.6(e) 3D crack propagation at Step 1745

It is observed that the micro-cracks appear everywhere within the cube other than only lie in some specific regions. The reason for this phenomenon is obvious, because the external force applied is a uniform tensile surface load in the vertical direction (z -direction) and no notch is made on the specimen, which results in a uniform tensile stress state at every point in the cube. Similar results can be found in [14] while using another approach. In [14], the micro-structure of cement paste is simulated by the NIST's 3D model (CEMHYD3D) [15] and solid element is adopted in the fracture analysis.

Furthermore, most of the micro-cracks concentrate at a certain region, because stress concentration occurs when the first micro-cracks have formed. These micro-cracks make up the main crack which might be observed in experiment.

Chapter 6 Results of Numerical Simulations

A set of numerical experiments are carried out to evaluate the numerical model developed in Chapter 3. All the examples in this chapter use the cube of cement paste in the dimension of $100\times100\times100mm^3$.

6.1 Tensile strength

The tensile strength of the specimen can be calculated on basis of the peak load in the load-displacement diagram.

6.1.1 Influence of curing age

Figure 6.1(a) and (b) show the tensile strength development against curing age and degree of hydration respectively. These results reflect the commonly known fact that tensile strength increases while the curing age and/or degree of hydration is increasing.

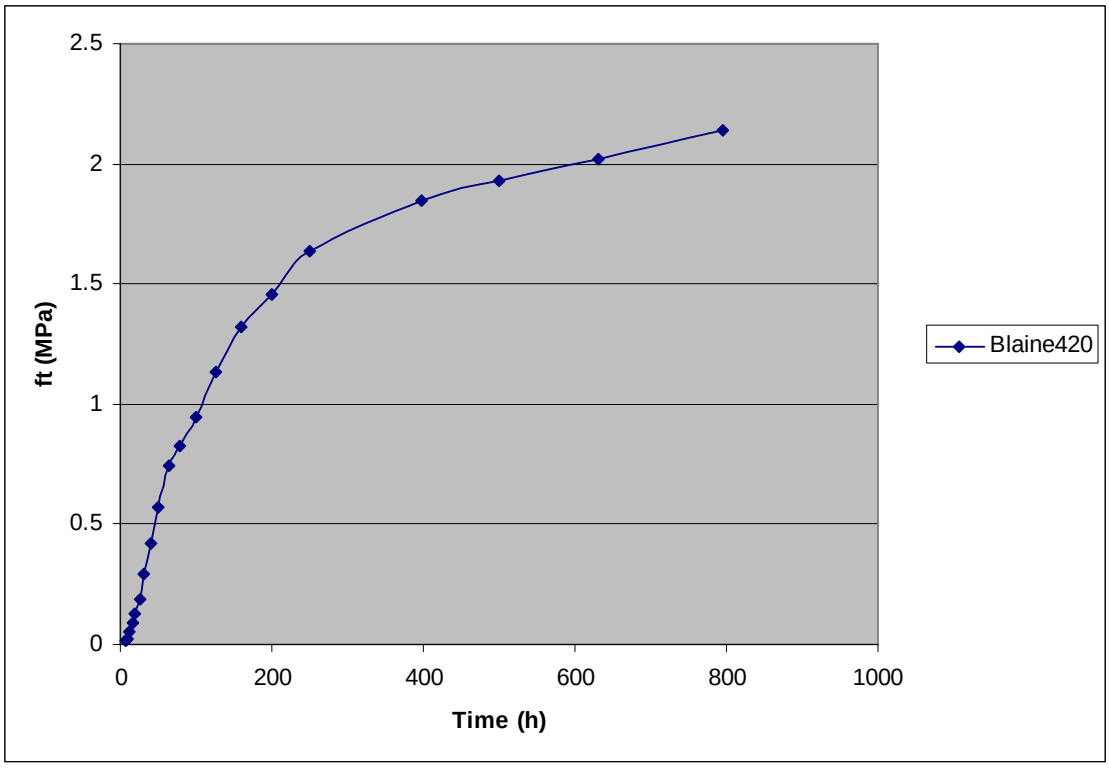

Figure 6.1(a) Tensile strength development against curing age

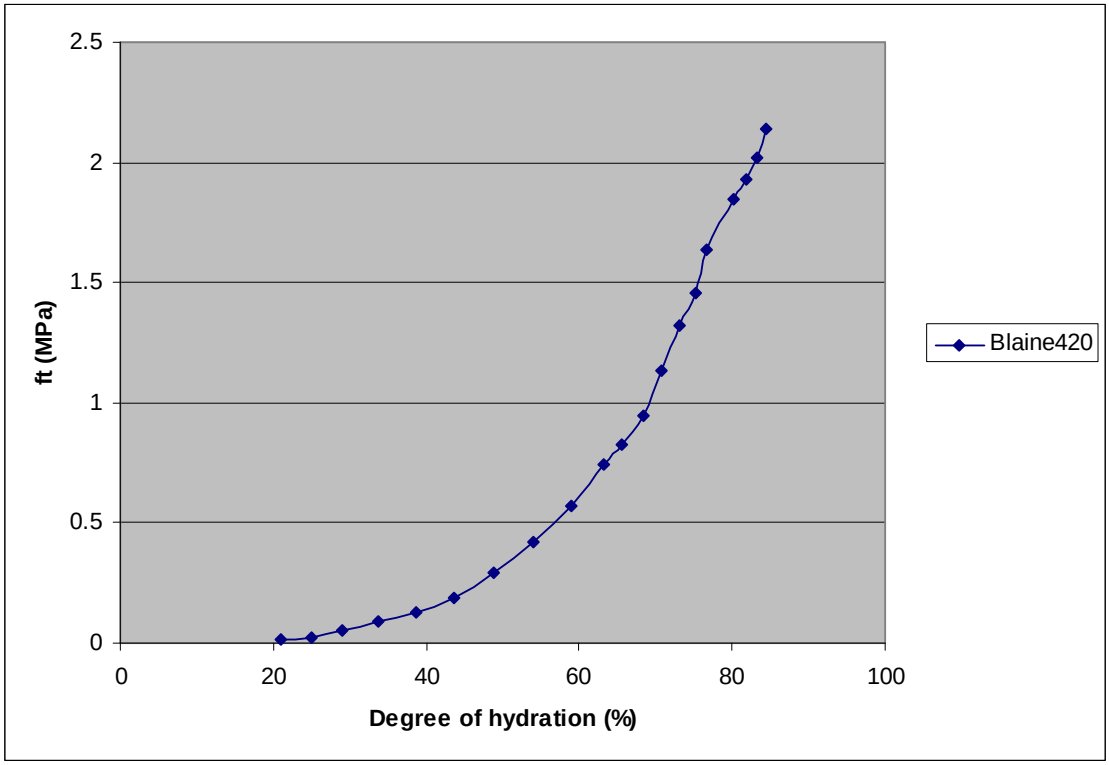

Figure 6.1(b) Tensile strength development against degree of hydration

6.1.2 Influence of Blaine value

Figure 6.2 demonstrates the tensile strength developments against curing age for different cements, the Blaine values of which are $420m^2/kg$ and $210m^2/kg$ respectively. Two general conclusions can be addressed from this figure,

(1) Finer cement can always has higher tensile strength compared with the one at the same curing age;

(2) The tensile strength of finer cement increases faster.

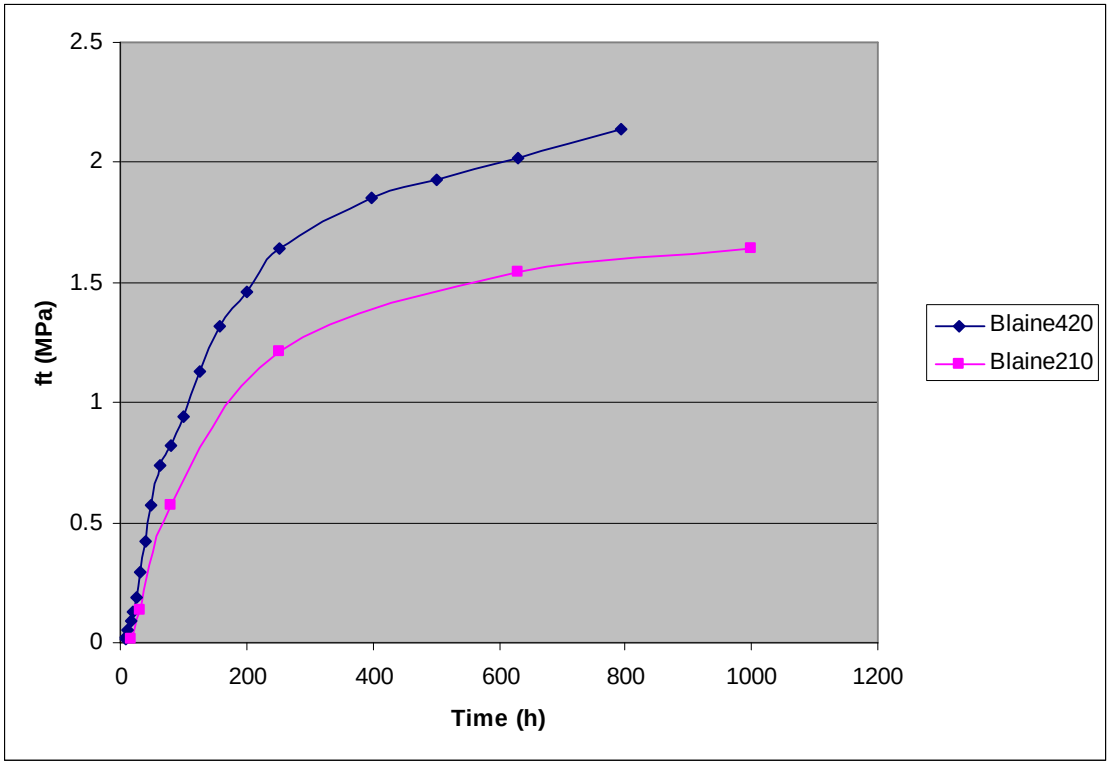

Figure 6.2 Tensile strength developments for different cements

6.2 Stiffness

The stiffness of the specimen can be calculated using the information in the load-displacement diagram. The slope of the curve in the linear stage illustrates the stiffness of the specimen.

6.2.1 Influence of curing age

Figure 6.3(a) and (b) show the stiffness development against curing age and degree of hydration respectively. These results reflect the commonly known fact that stiffness increases while the curing age and/or degree of hydration is increasing.

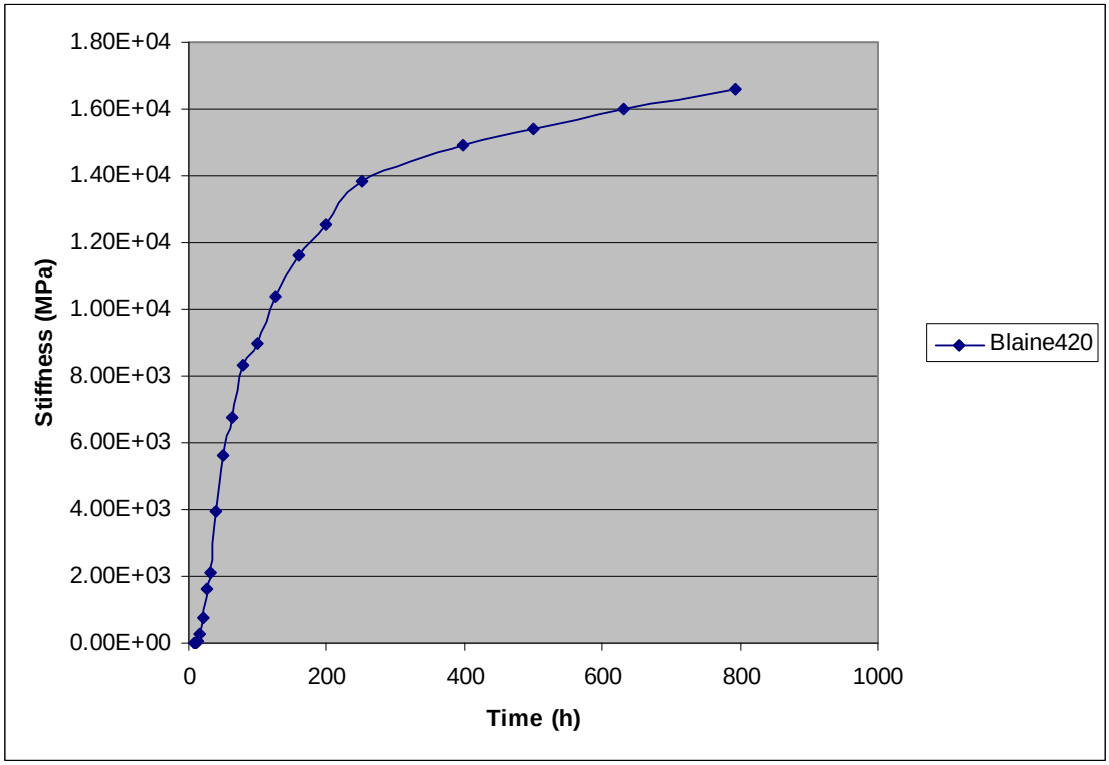

Figure 6.3(a) Stiffness development against curing age

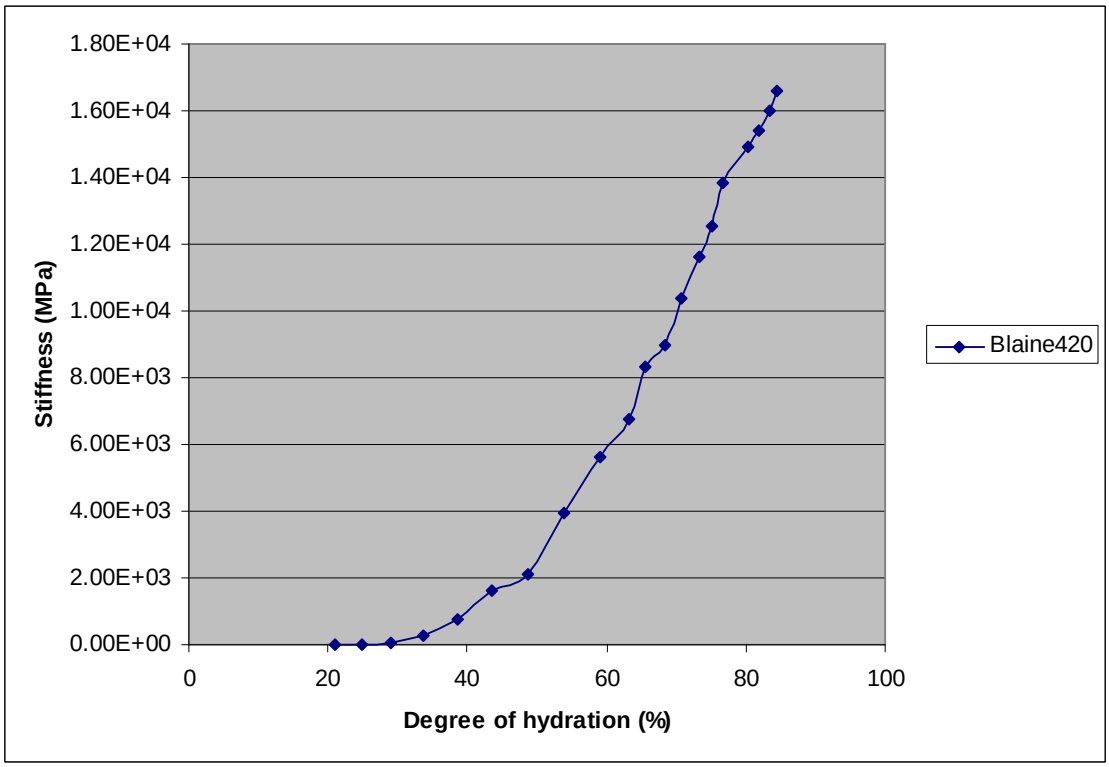

Figure 6.3(b) Stiffness development against degree of hydration

6.2.2 Influence of Blaine value

Figure 6.4 demonstrates the stiffness developments against curing age for different cements, the Blaine values of which are $420m^2/kg$ and $210m^2/kg$ respectively. Two general conclusions can be addressed from this figure,

(1) Finer cement can always has higher stiffness compared with the one at the same curing age;

(2) The stiffness of finer cement increases faster.

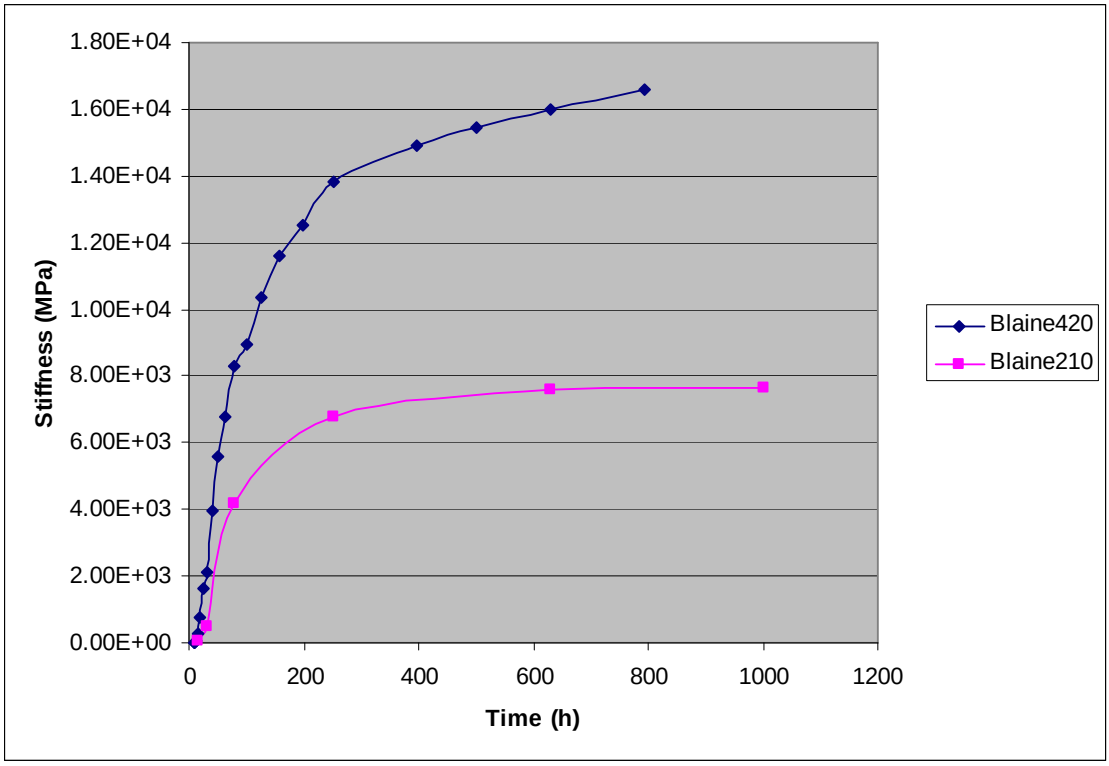

Figure 6.4 Stiffness developments for different cements

6.3 Relationship between tensile strength and stiffness

Figure 6.5 shows the relationship between tensile strength and stiffness for cement pastes with different curing ages. The Blaine value is fixed at $420m^2/kg$. This figure illustrates that the tensile strength of the system is almost proportional to its stiffness, and the coefficient is about 0.0001 which is equal to the one for local single element. This equality demonstrates that the proportional coefficient is independent of specimen size within the range $1mm \sim 100mm$.

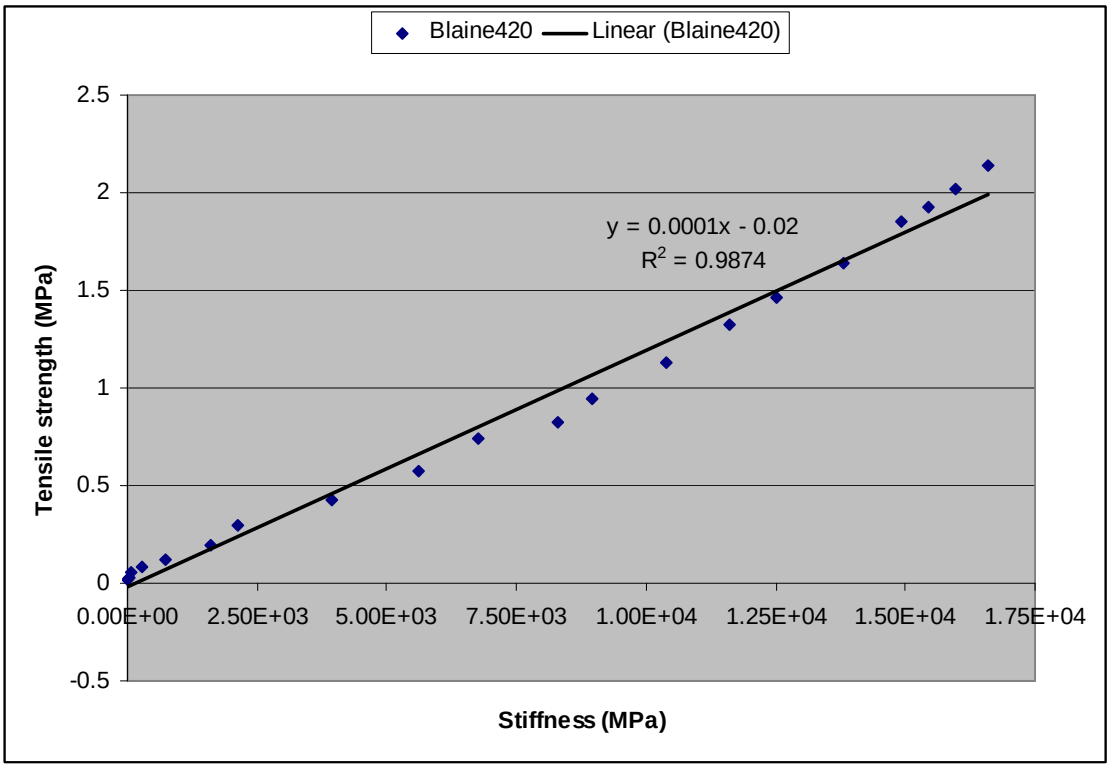

Figure 6.5 Relationship between tensile strength and stiffness for cement pastes

Chapter 7 Summary and Further Investigation

7.1 Summary of the MSc thesis project

In this MSc thesis project, an effort is made to predict the mechanical properties and crack propagation of cement paste using 3D lattice fracture model at the micro-level.

This project consists of three modules, namely 3D Lattice Generation, 3D Lattice Analysis and Interpretation of results, the role of which are pre-processing, kernel and post-processing according to Finite Element Method.

In the module "3D Lattice Generation", a lattice of beams is generated from micro-structure of cement paste which is one of the outcomes of hydration model HYMOSTRUC.

The following module "3D Lattice Analysis" simulates the fracture process of the cement paste due to uni-axial tensile load.

The last module "Interpretation of results" visualizes the results from 3D Lattice Analysis, the output of which is given in terms of load-displacement diagram and crack propagation images.

During the current investigation, only the influences of curing age and Blaine value are studied, while the influences of water/cement ratio and size effect are left for further research.

7.2 Known limitations and possible solutions

The proposed method for predicting mechanical properties and crack propagation of cement paste can be improved further in several aspects.

First of all, it is found that the simulation results for compression test are not in accordance with experiment observation so well [16]. It is suggested in [17] to remove the critical element by two steps instead of one step, where momentary resistance is removed first then the axial resistance.

Another drawback of the current implementation is that the demand for computational time is so huge that makes it impossible to get sufficient comparative results within a reasonable period. Parallel computing would be a good solution to this problem. A parallel implementation of 3D frame analysis is developed in [18], which is the fundamental of 3D lattice analysis.

7.3 Further investigation

In this research project, only cement paste is taken into account. However, the addressed principles must also hold for mortar and concrete. Moreover, the effect of hydration heat and shrinkage can also be incorporated by multi-scale approach.

References

[1] A. Neville, "Properties of concrete", 4th and Final Edition, (Addison Wesley Longman, 1995)

[2] D. Ngo and A. Scordelis, "Finite Element Analysis of Reinforced Concrete Beams", *J Am Concr Inst* 64 (1967) 152–163

[3] Y. Rashid, "Ultimate strength analysis of prestressed concrete pressure vessels", *Nuclear Engineering and Design* 7 (1968) 334–344

[4] R. de Borst and L. Sluys, "Computational Methods in Non-linear Solid Mechanics", CT5142 Lecture Notes, Delft University of Technology, (2007)

[5] E. Schlangen, "Experimental and Numerical Analysis of Fracture Processes in Concrete", PhD Thesis, Delft University of Technology, (1993)

[6] A. Hrennikoff, "Solution of problems of elasticity by the framework method", *Journal of Applied Mechanics* 12 (1941) 169–175

[7] K. van Breugel, "Simulation of Hydration and Formation of Structure in Hardening Cement-Based Materials", PhD Thesis (2nd Edition), Delft University of Technology, (1997)

[8] G. Ye, "The Microstructure and Permeability of Cementitious Materials", PhD Thesis, Delft University of Technology, (2003)

[9] L. Tan, "Failure Mechanisms in Hydrating Cement Particle Systems", MSc Thesis, Delft University of Technology, (2007)

[10] J. Shewchuk, "An Introduction to the Conjugate gradient Method without the Agonizing Pain", $1\frac{1}{4}$ Edition, Carnegie Mellon University, (1994)

[11] Y. Liu, W. Zhou and Q. Yang, "A distributed memory parallel element-by-element scheme based on Jacobi-conditioned conjugate gradient for 3D finite element analysis", *Finite Elements in Analysis and Design* 43 (2007) 494–503

[12] V. Smilauer and Z. Bittnar, "Microstructure-based micromechanical prediction of elastic properties in hydrating cement paste", *Cement and Concrete Research* 36 (2006) 1708–1718

[13] E. Schlangen and E. Garboczi, "Fracture simulations of concrete using Lattice models: Computational aspects", *Engineering Fracture Mechanics* Vol. 57, No. 2/3, (1997) 319–332

[14] F. Bernard, S. Kamali-Bernard and W. Prince, "3D multi-scale modeling of mechanical behaviour of sound and leached mortar", *Cement and Concrete Research* 38 (2008) 449–458

[15] D. Bentz, "CEMHYD3D: A Three-Dimensional Cement Hydration and Microstructure Development Modeling Package (Version 3.0)", National Institute of Standards and Technology Interagency Report, Technology Administration, U.S. Department of Commerce, NISTIR 7232, June 2005

[16] J. van Mier, A. Vervuurt and M. van Vliet, "Materials Engineering of Cement-Based Composites Using Lattice Models", WIT Press, Boston, Southampton, Computational Mechanics Publications, (1999) 1–32

[17] M. Abreu, J. Lemos, J. Carmeliet and E. Schlangen, "Modelling compressive cracking in concrete by a modified lattice model", in *New Trends in Fracture*

Mechanics of Concrete, Volume 1 of the Proceedings of the 6th International Conference on Fracture Mechanics of Concrete and Concrete Structures, Catania, Italy, June, 2007 (Taylor & Francis Group, London, UK, 2007) 453–460

[18] Z. Qian, "Parallel Implementation of 3D Frame Analysis", Additional MSc Thesis, Delft University of Technology, (2008)

Bibliography

(1) Becker, P., "The C++ Standard Library Extensions", (Addison–Wesley, 2007)

(2) Garboczi, E. and Day, A., "An algorithm for computing the effective linear elastic properties of heterogeneous materials: Three-dimensional results for composites with equal phase poisson ratios", *J. Mech. Phys. Solids*, Vol. 43, No. 9 (1995) pp. 1349–1362

(3) Hughes, T., Levit, I. and Winget, J., "An element-by-element solution algorithm for problems of structural and solid mechanics", *Computer methods in applied mechanics and engineering* 36 (1983) 241–254

(4) ISO/IEC Standard, "Programming languages–C++", 2nd Edition, ISO/IEC 14882:2003(E)

(5) Josuttis, N., "The C++ Standard Library: A Tutorial and Reference", (Addison–Wesley, 1999)

(6) Karlsson, B., "Beyond the C++ Standard Library: An Introduction to Boost", (Addison–Wesley, 2005)

(7) Leon, L. and Mishnaevsky, Jr., "Automatic voxel-based generation of 3D microstructural FE models and its application to the damage analysis of composites", *Materials Science and Engineering A* 407 (2005) 11–23

(8) Lippman, S., Lajoie, J. and Moo, B., "C++ primer", 4th Edition, (Addison–Wesley, 2005)

(9) Marti, R., Campos, V. and Pinana, E., "A branch and bound algorithm for the matrix bandwidth minimization", *European Journal of Operational Research* 186 (2008) 513–528

(10) Mattson, T., Sanders, B. and Massingill, B., "Patterns for Parallel Programming", (Addison–Wesley, 2005)

(11) Murugesan, K., Lo, D. and Young, D., "An efficient global matrix free finite element algorithm for 3D flow problems", *Commun. Numer. Meth. Engng* 21 (2005) 107–118

(12) Prata, S., "C++ Primer Plus", 5th Edition, (Sams, 2005)

(13) Quinn, M., "Parallel Programming in C with MPI and OpenMP", (McGraw–Hill Companies, 2004)

(14) Schlangen, E. and Garboczi, E., "New method for simulating fracture using an elastically uniform random geometry Lattice", *Int. J. Engng Sci.* Vol. 34, No. 10 (1996) pp. 1131–1144

(15) Schlangen, E., Koenders, E. and van Breugel, K., "Influence of internal dilation on the fracture behaviour of multi-phase materials", *Engineering Fracture Mechanics* 74 (2007) 18–33

(16) Simone, A., "Analysis of Slender Structures", CT3110 Lecture Notes, Delft University of Technology, (2007)

(17) Smith, I. and Griffiths, D., "Programming the Finite Element Method", 4th Edition, (John Wiley & Sons Ltd, England, 2004)

(18) Stroustrup, B., "The C++ Programming Language", Special Edition, (Addison–Wesley, 2000)

(19) Sun, Z., Ye, G. and Shah, S., "Microstructure and Early-Age Properties of Portland

Cement Paste–Effects of Connectivity of Solid Phases", *ACI Materials Journal*, V. 102, No. 2 (2005) pp. 122–129
(20) Tan, L., Schlangen, E. and Ye, G., "Simulation of Failure in Hydrating Cement Particles Systems", ***Key Engineering Materials*** Vols. 348–349 (2007) pp. 737–740
(21) Taylor, H., "Cement Chemistry", (Academic Press, 1990)
(22) Wells, G., "The Finite Element Method: An Introduction", CT5123 Lecture Notes, Delft University of Technology, (2006)

About the project

The MSc thesis project was started in September 2007 and completed in April 2008, which lasted for eight months.

This project was carried out at the Microlab, Faculty of Civil Engineering and Geosciences, Delft University of Technology, the Netherlands.

The committee members of this project are Prof. dr. ir. Klaas van Breugel, Dr. Guang Ye, Dr. ir. Erik Schlangen, Dr. ir. Pierre Hoogenboom and Ir. Lambert Houben.

The numerical model presented in this thesis was applied to make the computer program "3D Lattice Generation and Analysis", which was written in the programming language C++. All the source codes can be obtained upon request via the author's E-mail z.qian@msn.com